ELSEVIER

International Journal of Solids and Structures 41 (2004) 5463–5482

INTERNATIONAL JOURNAL OF SOLIDS and STRUCTURES

www.elsevier.com/locate/ijsolstr

On the dynamic propagation and arrest of buckles in pipe-in-pipe systems

S. Kyriakides [a,*], T.A. Netto [b]

[a] *Center for Mechanics of Solids, Structures and Materials, University of Texas at Austin, WRW 110, Austin, TX 78712, USA*
[b] *Universidade Federal do Rio de Janeiro, COPPE-Programa de Engenharia Oceanica, Caixa Postal 68508, Rio de Janeiro RJ 21945-970, Brazil*

Received 17 April 2004; received in revised form 17 April 2004
Available online 20 May 2004

Abstract

Experiments and large scale numerical simulations are used to study the dynamics and the arrest of propagating buckles in pipe-in-pipe systems. In the first set of experiments the velocity of buckles initiated in a constant pressure environment is measured as a function of pressure using first water and then air as pressurizing media. For the outer and inner pipe parameters used, the buckle velocities correlated well with values measured in single pipes. The dynamic propagation experiments in air were then simulated numerically. Calculated buckle velocities followed the same trend as the measured values although they were somewhat higher. In the second set of experiments the effectiveness of internal ring buckle arrestors designed with previously developed quasi-static design procedures is re-evaluated under dynamic buckle propagation. In all cases examined the dynamic arresting efficiency was found to be higher than the quasi-static one. The same behavior was also observed in corresponding numerical simulations. This indicates that design of such devices using quasi-static design criteria should be conservative.

Keywords: Pipe-in-pipe; Propagating buckles; Dynamic arrest

1. Introduction

Pipe-in-pipe systems are increasingly used in deepwater pipeline applications in which thermal insulation of the line is necessary. Typically, the annulus between the two pipes is either empty or contains non-structural insulation material. In deepwater applications such as ones of current interest in several parts of the world, the carrier pipe must be designed to resist collapse due to the ambient external pressure while the design of the inner pipe is primarily based on the pressure of the hydrocarbons it carries. The integrity of the two-pipe system in the event of accidental collapse of the carrier pipe is an issue of concern.

* Corresponding author. Tel.: +1-512-4714167; fax: +1-512-4715500.
E-mail address: skk@mail.utexas.edu (S. Kyriakides).

0020-7683/$ - see front matter © 2004 Elsevier Ltd. All rights reserved.
doi:10.1016/j.ijsolstr.2004.04.035

The problem has recently been investigated through an extensive experimental study involving 2-in. diameter carrier tubes with diameter-to-thickness (D/t) values of approximately 24, 21 and 16.7 and inner tubes of several diameters and wall thicknesses (Kyriakides, 2002b; Kyriakides and Vogler, 2002). In most cases examined, external pressure initially caused local collapse of the outer tube which in turn damaged the inner tube. Subsequently, the collapse propagated simultaneously collapsing both tubes as shown in Fig. 1. The propagation pressure of the two-tube system (P_{P2}) was established experimentally and resulted in the following empirical relationship for P_{P2}:

$$\frac{P_{P2}}{P_P} \approx 1 + C\left(\frac{\sigma_{oi}}{\sigma_o}\right)^{0.4}\left(\frac{D_i}{D}\right)\left(\frac{t_i}{t}\right)^2 \tag{1}$$

where the outer tube variables have no subscript, the subscript "i" indicates variables of the inner tube, σ_o is the tube yield stress, D the diameter, t the wall thickness, and P_P is the propagation pressure of the outer tube alone ($C = 1.095$).

In view of the potential danger of initiating propagating collapse in such systems, they must be protected with buckle arrestors. All buckle arrestors developed for single pipes are also available for use on the outer pipe in pipe-in-pipe systems. These include slip-on arrestors, clamped arrestors and integral arrestors (e.g. see Johns et al., 1978; Kyriakides and Babcock, 1980; Park and Kyriakides, 1997; Kyriakides et al., 1997; Langner, 1999; Kyriakides, 2002a). The presence of the annulus in pipe-in-pipe systems prompted the development of a new arrestor concept. It consists either of one single ring or of a series of shorter rings in a compact package which is placed in the annulus between the two pipes. The rings slip-fit into the outer pipe as shown in Fig. 2. The main advantage of this new concept is its simplicity as it requires neither welding nor grouting. The main design issues are to decide the length, thickness and grade of steel necessary for the internal ring to be an effective buckle arrestor for a given pipe-in-pipe system installed in a given water depth.

The effectiveness of this arrestor was demonstrated in a recent combined experimental and analytical study (Olso and Kyriakides, 2003). The study involved quasi-static buckle propagation, arrest and cross-

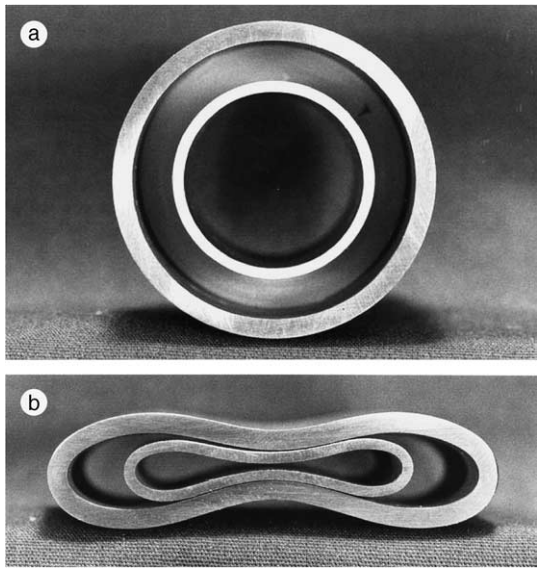

Fig. 1. Cross-section of pipe-in-pipe system: (a) initial and (b) after propagation of collapse.

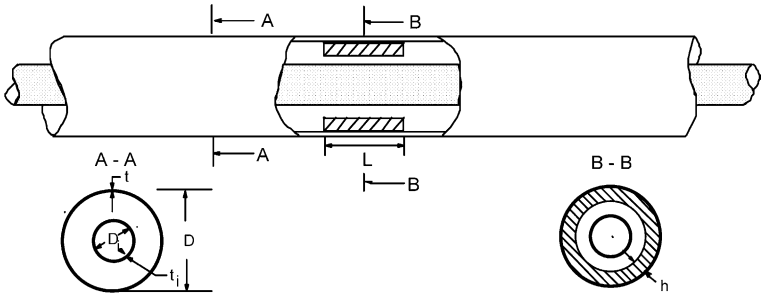

Fig. 2. Pipe-in-pipe system with an internal ring buckle arrestor.

over experiments similar to corresponding work on other arrestors. The results were used to develop an empirical design formula for the arresting efficiency of such devices defined by

$$\eta = \frac{P_X - P_P}{P_{CO} - P_P}, \quad 0 < \eta \leqslant 1 \tag{2}$$

where P_X is the arrestor crossover pressure, P_{CO} is the carrier pipe collapse pressure and P_P is the propagation pressure. The process of arrest and crossover was also simulated numerically with success. The main conclusion from the study was that such internal rings constitute a very effective means of arresting propagating buckles. For all cases considered, a combination of ring geometric and material parameters could be found so that the buckle could be held arrested until the collapse pressure of the downstream pipe was reached ($\eta = 100\%$).

On the sea floor the pressure is essentially constant and thus arrestors must stop buckles propagating at high velocities (Kyriakides and Babcock, 1979; Kyriakides and Netto, 2000). As a result, a quasi-static arrestor design must also be proven adequate under dynamic propagation conditions as was done for the slip-on (Kyriakides and Babcock, 1980) and integral arrestors (Netto and Kyriakides, 2000a,b).

In this paper we first present an experimental study on dynamic propagation of buckles in pipe-in-pipe systems in constant pressure environments (see also Kyriakides and Netto, 2002). The performance of internal ring arrestors designed with quasi-static criteria is then evaluated experimentally under dynamic propagation conditions. In the final section of the paper dynamic propagation and arrest experiments are simulated numerically and the results are used to explain the dynamic performance of the arrestors.

2. Experiments

2.1. Experimental set-up

The experimental set-up used to dynamically propagate buckles in small-scale pipe-in-pipe specimens is shown schematically in Fig. 3. The main facility is a 7 in. (178 mm) internal diameter, 13 ft (4 m) long pressure vessel with a pressure capacity of 9000 psi (620 bar). It can be pressurized with air or water. The pressure is monitored by an electrical pressure transducer and by pressure gages. The test specimens were seamless SS-304 tubes. The outer tubes had nominal diameter (D) of 1.75 in. (44.5 mm) and D/t of approximately 27. The inner tubes had nominal diameters (D_i) of 1.125 in. (28.6 mm) and two different diameter-to-thickness ratios: $D_i/t_i \cong 23$ and 32. Each test specimen consisted of two tubes held concentrically to each other by two polymeric centralizing rings placed close to the ends of the assembly. Both tubes were sealed with solid plugs, and the overall length of the assembly was around $38D$. Four strain

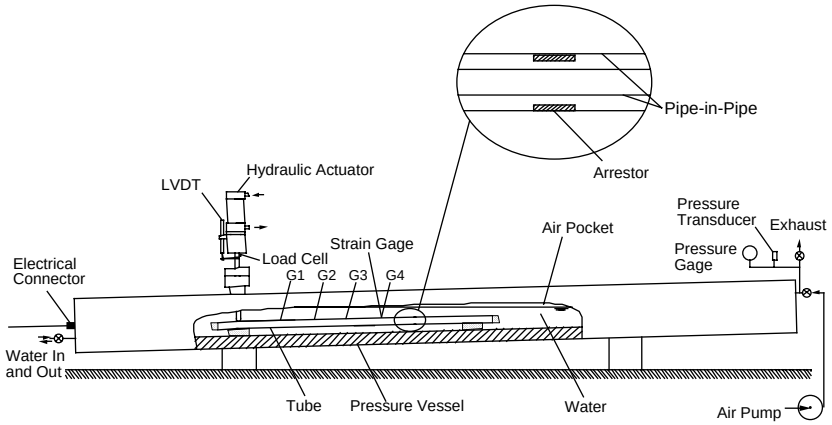

Fig. 3. Schematic of experimental set-up used for dynamic buckle propagation and arrest experiments.

gages (Gi, $i = 1, 4$) were mounted along the length of the carrier tube (see Fig. 3) for the purpose of registering the propagation of the collapse. The signals from these gages were later used to establish the velocity at which the buckle propagates. Strain gages and connecting wires were insulated with a compliant coating.

2.2. Dynamic buckle propagation in pipe-in-pipe systems

Dynamic collapse tests were performed with water as well as air as pressurizing media. The pressure vessel is positioned at a small angle to the horizontal and the test specimens were placed at the lower end of the vessel. When water was the pressuring medium, the vessel was filled with water leaving an air pocket which was subsequently pressurized by air supplied by air boosters. The size of the air pocket was large enough so that when the tube collapsed the pressure drop was less than 5% of the initial value. For air experiments, the vessel was directly pressurized with air.

Once the vessel pressure reached the desired level, a buckle was initiated by impacting one end of the tube with a rod connected to an external actuator shown in Fig. 3. The local collapse starts spreading, accelerates and reaches a steady-state velocity within a few tube diameters from the impact site and then propagates down the length of the tube. During the experiment signals from the pressure transducer, the load cell and LVDT of the impactor, and from the strain gages were recorded using a computer operated data acquisition system. In a typical dynamic test, data was acquired at a rate of 50,000 samples per second and saved on disk for later processing.

Fig. 4 shows a typical set of data from the four strain gages. This was recorded for a water experiment at a pressure of 1746 psi (120.4 bar). The change in local curvature, induced by the buckle profile as it travels along the tube, is reflected by the upper and lower voltage spikes seen in the figure. The time interval between the spikes from each strain gage is measured and by using the distances between the gages the buckle velocity is determined. In the experiment reported in the figure, the velocity between G1 and G2 was 717 ft/s (219 m/s), between G2 and G3 742 ft/s (226 m/s), and between G3 and G4 729 ft/s (222 m/s). The last value was taken as the steady-state velocity.

Fourteen dynamic collapse experiments on pipe-in-pipe specimens were conducted at initiation pressures (P_I) in the range $P_{P2} < P_I < P_{CO}$. In eight of these, water was the pressurizing medium and in six air. The measured steady-state velocities (U) are plotted in Figs. 5 and 6 against P_I. For the water experiments PIP1 and PIP2 refer to systems in which the inner tube had D_i/t_i of approximately 32 and 23, respectively.

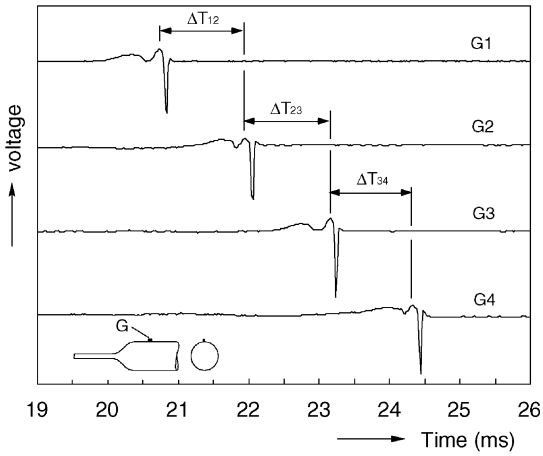

Fig. 4. Typical strain gage signals recorded in a dynamic experiment.

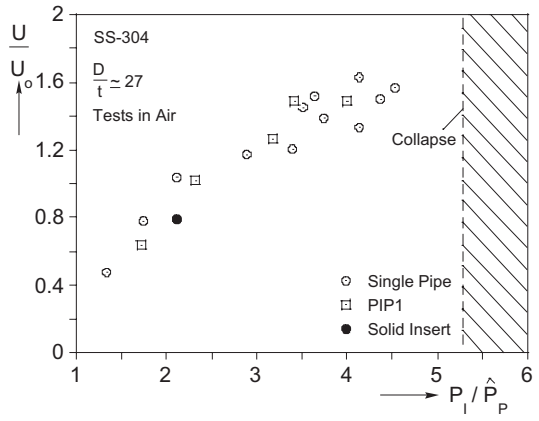

Fig. 5. Velocity of buckle propagation in air as a function of the external pressure.

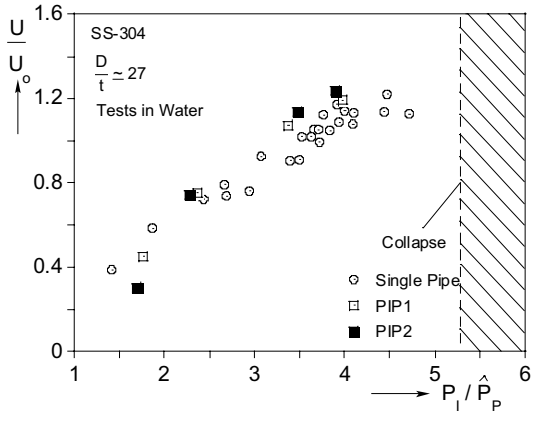

Fig. 6. Velocity of buckle propagation in water as a function of the external pressure.

Experimental results from similar experiments from Kyriakides and Netto (2000) on single tubes with the same nominal geometric and material parameters as those of the outer tubes are included in the plots (note that their actual D/t were approximately 28). Velocities are normalized by $U_o = \sqrt{\sigma_o/\rho}$, where σ_o is the measured yield stress of each outer tube and ρ is the material density (0.280 lb/in.^{3}—7750 kg/m^3). The initiation pressures (reported values are the average of the pressure at the start and at the end of the test) are normalized by the propagation pressure of each outer tube, estimated by the following empirical relationship:

$$\hat{P}_P = \sigma_o A \left(\frac{t}{D}\right)^{\beta} \tag{3}$$

where $A = 35.547$ and $\beta = 2.471$ (Dyau and Kyriakides, 1993). The main measured material and geometric parameters of the individual specimens tested in water and air are listed in Tables 1 and 2, respectively. The diameters and wall thicknesses represent the average values of sets of measurements made for outer and inner tubes.

The scatter seen in the plots can be attributed to small variations in the D/t, and the yield stress of the tubes used (the normalization reduces some of the scatter but not all of it). In both sets of experiments, no significant difference was observed between the buckle velocities in single tubes and pipe-in-pipe systems. In addition, in Fig. 6 the four tests with the thicker inner tube also fall in line with those of the thinner inner tube. Evidently, for the parameters of these pipe-in-pipe systems the presence of the inner tube does not change the dynamics of the problem significantly. In one air experiment conducted at $P_I = 896$ psi (61.8 bar) the inner tube was replaced by a solid rod with a diameter of 1.125 in. (28.6 mm). The buckle velocity is seen in Fig. 5 to again follow the trend of the rest of the results.

2.3. Dynamic performance of internal ring buckle arrestors

Design of buckle arrestors based on quasi-static procedures is a simpler, attractive alternative to the usually much more involved dynamic arrest experiments or analyses. In the case of the *slip-on* (Kyriakides and Babcock, 1979) and the *integral arrestors* (Netto and Kyriakides, 2000a,b) it was shown that the quasi-static design criteria are conservative; in other words, the crossover pressure of a given arrestor is higher when the buckle is running. For example, in the case of the integral arrestor this enhancement in performance by dynamics is related to the differences between the profiles of buckles propagating quasi-statically and dynamically (Netto and Kyriakides, 2000b). In the case of the slip-on arrestor the enhancement is

Table 1
Buckle velocities at various pressures for pipe-in-pipe experiments in air

D/t	σ_o ksi (MPa)	D_i/t_i	σ_{oi} ksi (MPa)	P_I psi (bar)	U/U_o	$P_I/\hat{P}_P$
26.12	39.18 (270.2)	32.47	43.68 (301.2)	752 (51.9)	0.635	1.713
26.38	38.9 (268.3)	S[a]	–	896 (61.8)	0.788	2.107
26.20	40.29 (277.9)	32.47	43.68 (301.2)	1003 (69.2)	1.020	2.315
28.22	45.37 (312.9)	33.02	47.31 (326.3)	1334 (92.0)	1.2636	3.178
26.12	39.18 (270.2)	32.57	43.68 (301.2)	1501 (103.5)	1.487	3.418
26.16	39.18 (270.2)	31.35	44.22 (305.0)	1749 (120.6)	1.487	4.000

[a] Solid rod.

Table 2
Buckle velocities at various pressures for pipe-in-pipe experiments in water

D/t	σ_o ksi (MPa)	D_i/t_i	σ_{oi} ksi (MPa)	P_I psi (bar)	U/U_o	$P_I/\hat{P}_P$
26.24	40.29 (277.9)	23.04	43.43 (299.5)	759 (52.3)	0.301	1.700
26.16	38.63 (266.4)	31.28	44.58 (307.4)	760 (52.4)	0.449	1.762
26.24	40.29 (277.9)	23.04	43.43 (299.5)	1019 (70.3)	0.742	2.273
26.16	38.63 (266.4)	31.45	44.58 (307.4)	1021 (70.4)	0.753	2.368
25.81	38.63 (266.4)	31.50	44.22 (305.0)	1501 (103.5)	1.073	3.368
26.19	38.9 (268.3)	23.03	43.43 (299.5)	1505 (103.8)	1.137	3.477
26.12	39.18 (270.2)	31.36	44.58 (307.4)	1746 (120.4)	1.190	3.976
26.24	38.9 (268.3)	23.23	46.34 (319.6)	1680 (115.9)	1.235	3.897

related to the more complex way a running buckle engages the ring arrestor. These enhancing mechanisms are specific to the two arrestor designs and cannot be simply inferred to other types of arrestors. Thus, the performance of internal ring buckle arrestors proposed by Olso and Kyriakides (2003) must also be proven under dynamic propagation conditions. For this reason, several arrestors designed by the quasi-static procedure of Olso and Kyriakides were evaluated dynamically. The pipe-in-pipe specimens used in these experiments were nominally identical to the ones used in the dynamic buckle propagation experiments reported above.

Three ring arrestors with the same length ($L = 0.5D$) and different thicknesses (h) were designed to have quasi-static arresting efficiencies between approximately 0.5 and 0.75. The rings were installed inside pipe-in-pipe systems. The main geometric and material parameters of the arrestors and tubes tested are given in Table 3. Their quasi-static crossover pressures (P_{XS}) were first determined as follows. The outer tube was first dented at one end before pressurization. The specimen was placed inside the vessel which was subsequently completely filled with water. The system was then pressurized using a positive displacement water pump. A typical pressure–time history recorded in such an experiment is shown in Fig. 7a. The pressure initially rises sharply with time until the dented section collapses (see ① in Fig. 7b); collapse is accompanied by a sudden drop in pressure. Because of the high stiffness of the pressure system, collapse is limited and further spreading requires additional supply of water into the system. The pressure stops dropping when the walls of the collapsed section come into contact. Subsequently, collapse starts to spread quasi-statically

Table 3
Parameters of tubes and internal arrestors tested quasi-statically ($L/D = 0.5$)

Arrest. no.	D/t	σ_o ksi (MPa)	D_i/t_i	σ_{oi} ksi (MPa)	h/t	Mode	P_{XS} psi (bar)	η_S
IA1	28.08	45.37 (312.9)	32.69	47.31 (326.3)	1.929	⬭	1301 (89.7)	0.4930
IA3	28.24	42.63 (294.0)	33.01	47.31 (326.3)	2.100	⬭	1503 (103.7)	0.6287
IA2	28.19	45.37 (312.9)	32.68	47.31 (326.3)	2.258	⬭	1724 (118.9)	0.7601

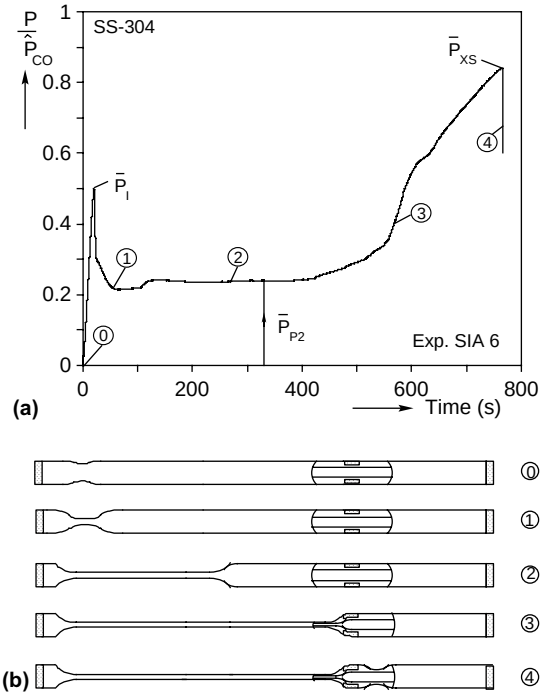

Fig. 7. Quasi-static propagation, arrest and crossover in a pipe-in-pipe system with an internal ring arrestor: (a) pressure–time history and (b) deformed configurations.

along the length of the tube towards the arrestor (②). The pressure plateau traced represents the propagation pressure of the two-tube system ($P_{P2} = 487$ psi—33.6 bar). This value is approximately 16% higher than the propagation pressure of the outer tube alone, estimated using Eq. (3). The collapse affects both tubes as shown in Fig. 1. The buckle is arrested when it engages the arrestor (see ③ in Fig. 7b). The pressure rises again until at 1724 psi (118.9 bar) the buckle crosses the arrestor and continues to propagate downstream of it (configuration ④ in Fig. 7b). In this test, the arrestor and the downstream segments of tubes ovalized and collapsed in the same sense as the upstream segment (flattening mode of crossover). The highest pressure recorded is the quasi-static crossover pressure of the arrestor (P_{XS}) which corresponds to an arresting efficiency $\eta_S = 0.76$.

Propagation pressures, crossover pressures and quasi-static efficiencies of the other arrestors used in this study are listed in Table 3. The schematic (⌔) represents the flattening mode of crossover shown in Fig. 8a. This mode was observed in all quasi-static experiments. Fig. 8b shows the flipping mode of crossover which occurred in two of the dynamic experiments depicted in Table 4 as (0).

The dynamic efficiencies of the same arrestors were subsequently established as follows. Several ring arrestors were machined for each of three efficiencies. Each ring was placed inside a similar pipe-in-pipe system which had a length of 45D. Each assembly was then tested dynamically in water as described in the previous section. Once initiated, a buckle quickly accelerated to a steady-state velocity and engaged the arrestor. The buckle was either arrested or it crossed the arrestor. In cases in which the buckle was arrested a new experiment was conducted with the same test specimen characteristics but at a pressure level of about 100 psi (7 bar) higher. Again we were looking for a cross/no cross result. This was repeated until the arrestor was eventually crossed. Typically the first test was conducted at a pressure level equivalent to P_{XS} and in all cases the buckles were arrested. In the three sets of experiments conducted 3–5 experiments were

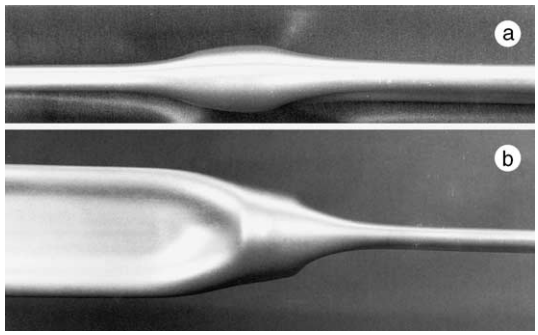

Fig. 8. Modes collapse crosses internal ring arrestors: (a) the flattening mode and (b) the flipping mode.

Table 4
Parameters of tubes and internal arrestors tested dynamically in water ($L/D = 0.5$)

Arrest. no.	D/t	σ_o ksi (MPa)	D_i/t_i	σ_{oi} ksi (MPa)	h/t	Mode[a]	P_I psi (bar)	η_D
IA1	28.02	46.74 (322.3)	32.72	40.07 (276.3)	1.923	–	1604 (110.6)	0.6818
IA1	27.81	47.38 (326.8)	32.81	40.07 (276.3)	1.917	O	1735 (119.7)	0.7626
IA2	27.85	47.38 (326.8)	32.71	40.07 (276.3)	2.233	–	1846 (127.3)	0.8337
IA2	27.79	47.38 (326.8)	32.62	40.74 (281.0)	2.228	O	1990 (137.2)	0.9257
IA3	28.34	42.63 (294.0)	32.71	40.74 (281.0)	2.114	–	1702 (117.4)	0.7526
IA3	28.44	42.63 (294.0)	32.71	40.74 (281.0)	2.120	O	1800 (124.1)	0.8130

[a] The symbol (–) indicates that no crossover occurred.

required before the dynamic crossover pressure (P_{XD}) was established (within 100 psi). For example, in the case of arrestor IA1 with $P_{XS} = 1301$ psi (89.7 bar), dynamic buckles were arrested up to a pressure of 1604 psi (110.6 bar). The buckle crossed the arrestor when the pressure was set at 1735 psi (119.6 bar).

For each arrestor, we report in Table 4 the highest pressure at which the buckle was arrested and the lowest pressure at which the buckle crossed the arrestor. The initiation pressure (P_I) listed is the average between the pressures at the beginning and at the end of each test (difference between the two was less than 5%). The main geometric and material parameters of the tubes and arrestors used in the tests are also given in Table 4. The propagation pressure of each specimen ($\hat{P}_{P2}$) was estimated using Eq. (1). This value was used to calculate the dynamic arresting efficiencies (η_D) listed in the table. One common value of collapse pressure ($\hat{P}_{CO} = 2106$ psi—145.3 bar) was adopted in all calculations of η. This value was calculated using the average values of the geometric and material parameters of all outer tubes used in this study using the custom computer program BEPTICO (Kyriakides et al., 1994).

The dynamic efficiencies measured are plotted against the corresponding quasi-static values in Fig. 9. In all cases, the dynamic efficiency is higher than the quasi-static value. Furthermore, the results indicate that arrestors with medium level efficiencies ($0.4 < \eta_S < 0.6$) experience a higher increase in performance under dynamic buckle propagation than higher efficiency arrestors. For two of the arrestors the dynamic mode of crossing switched from the flattening to the flipping mode. The same trend was observed by Netto and

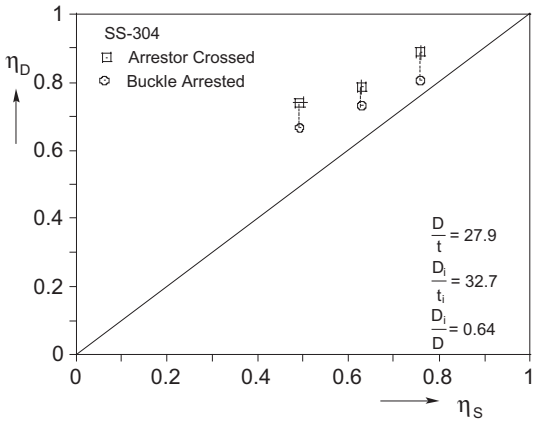

Fig. 9. Dynamic vs. quasi-static arresting efficiencies measured.

Kyriakides (2000a,b) for integral buckle arrestors. The reasons behind this dynamic enhancement in arresting efficiency will be discussed in the next section in the light of numerical results.

3. Analysis

The model used for the dynamic problem is an extension of the quasi-static models of pipe-in-pipe of Kyriakides and Vogler (2002) and Olso and Kyriakides (2003). It operates within the framework of the nonlinear FE code ABAQUS (version 6.3). The geometry of the model, shown in Fig. 10, consists of two concentric pipes with the characteristics given in Table 5. An arrestor of length L and thickness h is placed in the annulus and is in smooth contact with the inner wall of the outer pipe. The upstream section of the

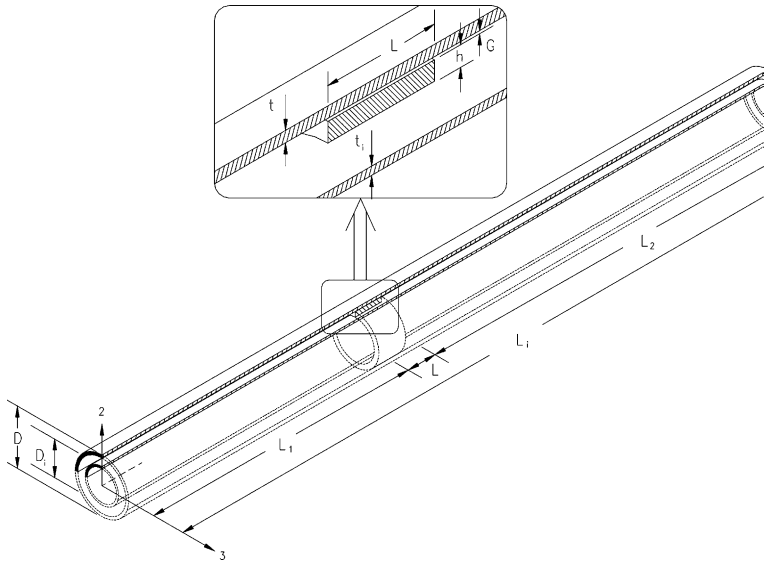

Fig. 10. Geometry of FE model of pipe-in-pipe with internal ring arrestor.

Table 5
Pipe-in-pipe and arrestor geometric and material properties used in analyses

D in. (mm)	D/t	E msi (GPa)	σ_o ksi (MPa)	D_i in. (mm)	D_i/t_i	E_i msi (GPa)	σ_{oi} ksi (MPa)	L/D	E_a msi (GPa)	σ_{oa} ksi (MPa)
1.752 (44.51)	26.63	29.8 (205)	40.64 (280.3)	1.126 (28.61)	32.36	29.8 (205)	44.51 (307.0)	0.5	26.4 (182)	41.21 (307.0)

$\hat{P}_{CO} = 2290$ psi (157.9 bar), $\hat{P}_{P2} = 530$ psi (36.6 bar).

system has length L_1 and the downstream section has length L_2. Guided by the pipe deformation seen in the experiments, planes 1–2 and 1–3 are assumed to be planes of symmetry. Plane 2–3 is also assumed to be a plane of symmetry. Collapse is initiated from a local imperfection in the outer pipe placed in the neighborhood of $x_1 = 0$. The imperfection has the form

$$w_0(\theta) = -\Delta_0 \exp\left[-\beta\left(\frac{x_1}{D}\right)^2\right]\cos 2\theta \tag{4}$$

where w_0 is the radial displacement and θ is the polar angular coordinate measured from the x_2-axis. The amplitude of the imperfection is Δ_0 and β decides its extent which typically was one to two pipe diameter long.

The pipes and the internal arrestors are discretized by three-dimensional, 27-node quadratic brick elements (C3D27). The appropriate number of elements in the radial (thickness), circumferential, and longitudinal directions were established by convergence studies. The dynamic problem is very large, each ran taking upwards of two weeks to perform. For this reason the convergence studies were performed for quasi-static buckle propagation which is considerably shorter. A non-uniform discretization in the circumferential direction was adopted such that regions where higher strain gradients are expected were more refined. The result of this study is a coarser version of the mesh used in Olso and Kyriakides (2003). It was assumed to be also satisfactory for the dynamic problem. The mesh has one element through the thickness of the pipes and two through the thickness of the arrestor. For all three components the elements have the following angular spans starting from the x_2-axis: 10°–10°–15°–15°–10°–10° –7.5°–7.5°–2.5°–2.5°. In the axial direction the upstream section of the outer pipe has 10 $1.0D$ long elements, followed by two $0.25D$ long elements in the arrestor region. In the downstream section, five $1.0D$ long elements were used.

Since only one quarter of the model was analyzed, a rigid surface was placed along the symmetry plane 1–3 using rigid elements (R3D4) to simulate contact of the inner wall of the inner pipe during propagation of collapse. Contact between inner and outer pipes and between inner pipe and the rigid elements along plane 1–3 was simulated by using surface-based hard-contact modeling. This model prevents penetration between contact surfaces. Additionally, no separation is allowed between surfaces that eventually come into contact.

External pressure is applied as a uniformly distributed load on the external faces of the elements that define the outer pipe (using DLOAD option in ABAQUS library). For experiments in air the added mass of the pressurizing medium is considered to be negligibly small and is not accounted for in the dynamic model.

The materials of the two pipes and the arrestor are modeled as elastic/powerlaw viscoplastic solids following the same framework developed in Netto and Kyriakides (2000b). For the uniaxial setting the inelastic strain rate is given by

$$\dot{\varepsilon}^p = D\left(\frac{\sigma}{\Sigma(\varepsilon^p)} - 1\right)^{m'} \tag{5}$$

where $\Sigma(\varepsilon^p)$ is the flow stress measured at a low base strain rate test. The shape of the base response is represented by a multilinear fit given in Fig. 2 of the reference. The yield stress is adjusted to correspond to the values in Table 5 while $D = 80 \times 10^3$ and $m' = 5$ (see Fig. 15, Netto and Kyriakides, 2000a).

3.1. Dynamic buckle propagation in pipe-in-pipe systems

We first consider the initiation and dynamic propagation of collapse in a pipe-in-pipe system in the absence of an arrestor. The model consists of two concentric pipes 20D long with the symmetries described above. The mesh has 21 equally spaced elements along the length, one through the thickness of each pipe and the circumferential distribution given above. The pipe is initially loaded quasi-statically by external pressure until local collapse is initiated. Riks' path following scheme is used to track the loading history over the pressure maximum. When the pressure drops to the level chosen for the dynamic run, it is fixed and a switch is made to the dynamic version of the model. The last equilibrium solution of the quasi-static analysis is given a small perturbation (usually, a small radial displacement at the crown point of the outer pipe at $x_1 = 0$), and the dynamic analysis is commenced. The overall equations of motion correspond to adding d'Alambert forces to the Principle of Virtual Work. The equations of motion are then integrated in time using the implicit operator of Hilber et al. (1977) and Hilber and Hughes (1978), as described in Netto and Kyriakides (2000b).

Fig. 11 shows a comparison of pressure–change in volume (P–$\delta\upsilon$) responses from such a dynamic calculation and from a corresponding one conducted quasi-statically. In the quasi-static case (solid line) the loading is conducted under volume control using the hydrostatic fluid elements of ABAQUS (a combination of F3D3 and F3D4). The pipe buckles locally at the site of the imperfection at a pressure somewhat lower than the collapse pressure of the intact geometry. The pressure drops until the walls of the inner pipe come into contact. Subsequently collapse propagates in a steady-state manner at the propagation pressure of the two pipe system P_{P2} which is at the level of 530 psi (36.6 bar—see Kyriakides and Vogler, 2002 for more details). In the dynamic case (dashed line), the initial localization of collapse is also conducted quasi-statically. P_I represents the level at which the pressure was fixed and the dynamic calculation was commenced. In this case collapse proceeds dynamically until the walls of the inner pipe in the neighborhood of $x_1 = 0$ come into contact. It then starts propagating down the pipe and quickly accelerates to a steady state (reaches steady–state at a distance of about 3D from the initiation site). In the process the profile of the collapsing front sharpens.

Such dynamic simulations were conducted at several pressure levels. Resultant steady-state velocities are listed in Table 6. The predicted velocities are compared to the values measured in the air experiments in Fig. 12. The predictions follow the trend of the measurements but they are generally somewhat higher. The size of these dynamic calculations is quite significant. As a result, the meshing scheme used was somewhat conservative and was not optimized. We consider this to be the main contributor to the over prediction of

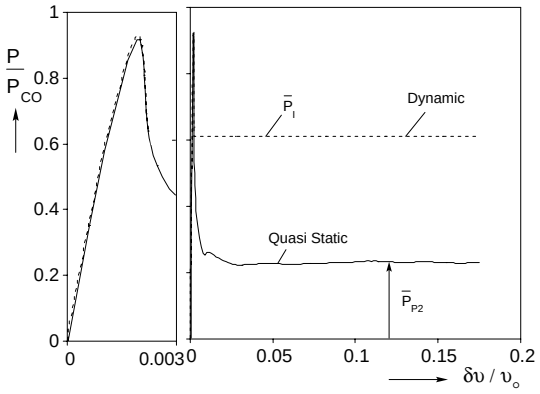

Fig. 11. Simulated pressure–change in volume responses for quasi-static and dynamic buckle propagation in a pipe-in-pipe system.

Table 6
Calculated buckle velocities at various pressure levels

P_I psi (bar)	$P_I/\hat{P}_P$	$P_I/\hat{P}_{P2}$	$\hat{U}/U_o$
750 (51.7)	1.726	1.415	0.923
1000 (68.97)	2.301	1.887	1.317
12.50 (86.21)	2.877	2.358	1.502
1500 (103.4)	3.452	2.830	1.593

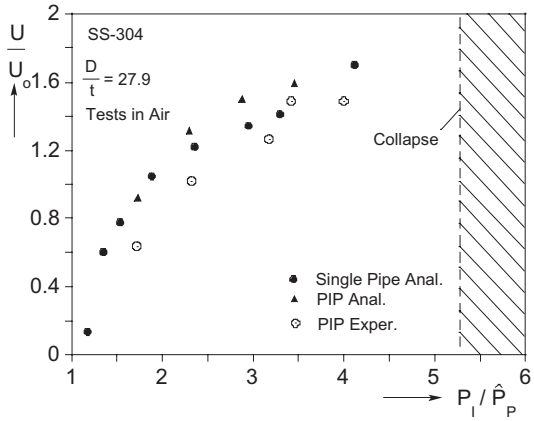

Fig. 12. Comparison of buckle velocities measured in air experiments and predicted values for buckles propagating in vacuum.

the buckle velocities. Included in the figure are the velocities predicted for a similar set of single pipes from Kyriakides and Netto (2000). These also follow the same trend and are close to the velocities predicted for the pipe-in-pipe system. This confirms the experimental observation that for this combination of pipe-in-pipe parameters, the presence of the inner pipe had a small effect on the buckle velocities.

It was previously shown that in single pipes the profile of the propagating collapse gets sharper as the velocity increases (Fig. 18 in Kyriakides and Netto, 2000). Indeed, this plays a role in the dynamic enhancement of integral arrestors. The sharpening is nonlinearly dependent on velocity as it saturates at higher velocities. Fig. 13a shows a comparison of the shape of the most deformed generator of the outer pipe in our pipe-in-pipe system at four different velocities as well as for quasi-static propagation. The length of the deformed generators is representative of the profile length. The sharpening of the profile as the buckle velocity increases is quite clear. However, the profiles at the two higher velocities do not show much difference as was the case in the single pipe. A quantitative presentation of the change of the profile length with pressure is shown in Fig. 14. At $P_I/\hat{P}_{P2} = 2.83$ the profile length is down to one half the length at quasi-static propagation. This trend is similar to that seen in single pipes although for the pipe-in-pipe the profiles are somewhat longer at the same pressure levels.

Fig. 13b shows expanded views of the radial displacements of the same generator for the quasi-static case and for the dynamic cases corresponding to $P_I/\hat{P}_{P2} = 2.83$ and 1.89. All three show that just ahead of the propagating collapse profile there exists a zone of outward deflection. These are zones where the cross-section ovalizes with its major axis orthogonal to the axis of collapse upstream. Their span is approximately

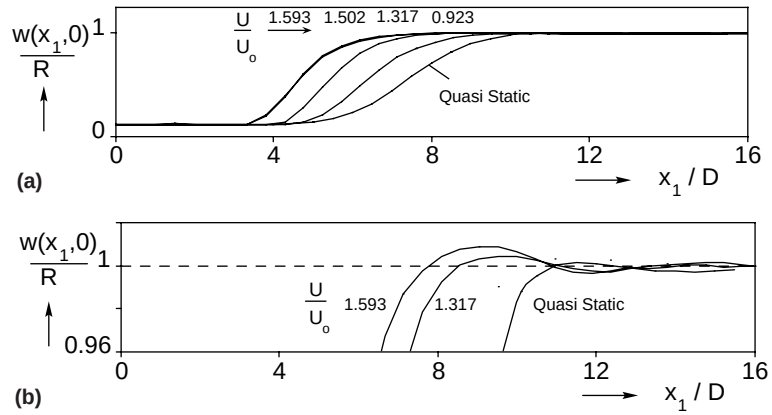

Fig. 13. (a) Comparison of deformed contours of outer pipe generator $(x, 0)$ for the quasi-static and four dynamic solutions at increasing velocities. (b) Expanded views of three of the generators showing reverse ovalization ahead of the buckle fronts.

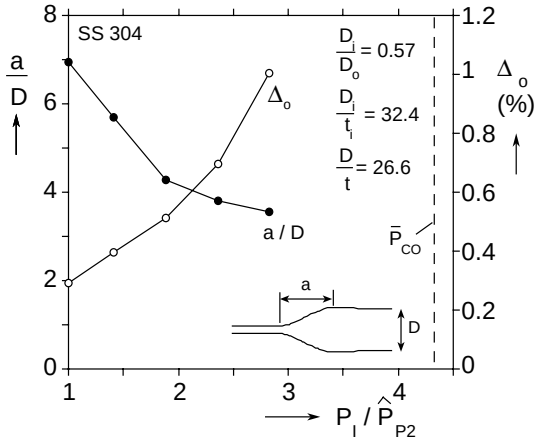

Fig. 14. Calculated buckle profile lengths and maximum amplitude of corresponding induced reverse ovality as a function of pressure.

4D long. The maximum amplitude of reverse ovality, Δ_0, is plotted against the pressure in Fig. 14. It is seen to increase with pressure (and velocity) quite significantly. For the quasi-static case it is 0.29% while at $P_I/\hat{P}_{P2} = 2.83$ it reaches a level of 1.0%. This increase in ovality is due to the sharpening of the buckle profile induced by inertial effects. We remind the reader that at even higher pressures the reverse ovality will cause the flip–flop mode of collapse to take place as was reported for single pipes (Kyriakides and Netto, 2000).

3.2. Dynamic buckle arrest in pipe-in-pipe systems

We now consider pipe-in-pipe systems with internal ring arrestors. As in the experiments, the quasi-static crossover pressure of each arrestor is established first. Such calculations are again performed under volume control. Fig. 15 shows the pressure–change in volume (P–δv) response from a representative case. The pipe-in-pipe parameters are the same as above while the arrestor is 0.5D long and its thickness h is 1.8237t. Fig. 16 displays the initial and a sequence of model deformed configurations corresponding to the points

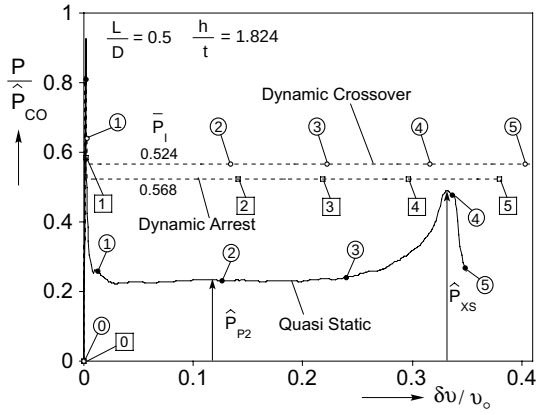

Fig. 15. Pressure–change in volume response of pipe-in-pipe with arrestor from dynamic calculations at two pressure levels and corresponding quasi-static response.

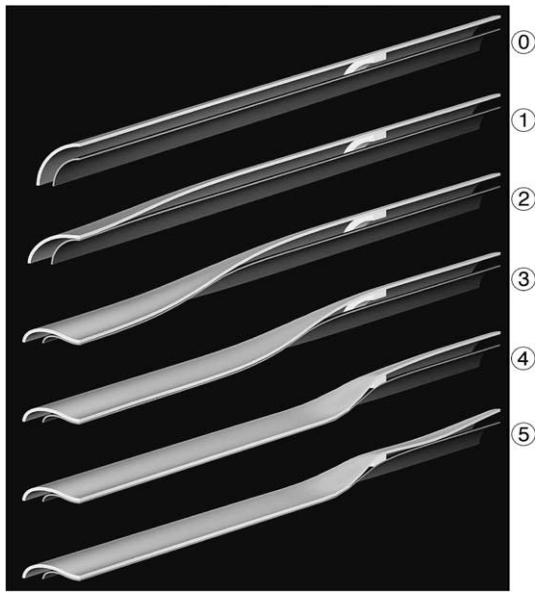

Fig. 16. Sequence of calculated deformed configurations corresponding to points identified on quasi-static response in Fig. 15.

marked with numbered flags on the response. The initial part of the response, corresponding to local collapse and steady-state propagation of collapse (configurations ① and ②), is the same as in Fig. 11. Steady-state propagation is halted when the collapse engages the arrestor (③). The pressure increases causing the collapsed pipes behind the arrestor to flatten further while downstream of the arrestor the outer pipe starts to ovalize (④). Eventually the pressure and the ovalization reach a critical combination causing the downstream section of pipe to collapse. As evidenced by configuration ⑤, this arrestor is crossed via the flattening mode. The crossover pressure ($\hat{P}_X$) is 1118 psi (77.1 bar).

The propagation pressure of this pipe-in-pipe system ($\hat{P}_{P2}$), corresponding to the plateau value in Fig. 15, is 530 psi (36.6 bar). The collapse pressure of the intact outer pipe with a uniform ovality of 0.1% is 2290 psi

(157.9 bar). Using these values and the calculated crossover pressure Eq. (2) yields the quasi-static arrestor efficiency ($\hat{\eta}_S$) to be 0.334. Similar calculations were performed for three other arrestors with the same length and the thicknesses listed in Table 7. The recorded crossover pressures and arresting efficiencies are also listed in Table 7. All four arrestors were crossed via the flattening mode.

Dynamic calculations on models with internal ring arrestors follow the same initiation procedure outlined in the previous section. The dashed lines in the (P–δv) plot in Fig. 15 correspond to such dynamic calculations performed at two different pressure levels. Sequences of deformed configurations corresponding to the two calculations are shown in Figs. 17 and 18. In the first calculation, the pressure was set 1200 psi (82.7 bar) or 82 psi (5.6 bar) higher than the quasi-static crossover pressure. Collapse localized (1 in Fig. 17), propagated dynamically reaching steady state (2 and 3), engaged the arrestor (4), was arrested, and came to rest (5). In the next calculation the pressure was increased to 1300 psi (89.6 bar). The sequence of configurations shown in Fig. 18 is similar but at this pressure level, the buckle crossed the arrestor via the flattening mode. Thus, the actual dynamic crossover pressure is between 1200 and 1300 psi

Table 7
Calculated quasi-static arrestor efficiencies ($L/D = 0.5$)

h/t	Mode	$\hat{P}_{XS}$ psi (bar)	$\hat{\eta}_S$
1.8237	⬭	1118 (77.1)	0.334
1.9757	⬭	1225 (84.5)	0.395
2.1277	⬭	1415 (97.6)	0.503
2.2796	⬭	1598 (110.2)	0.607

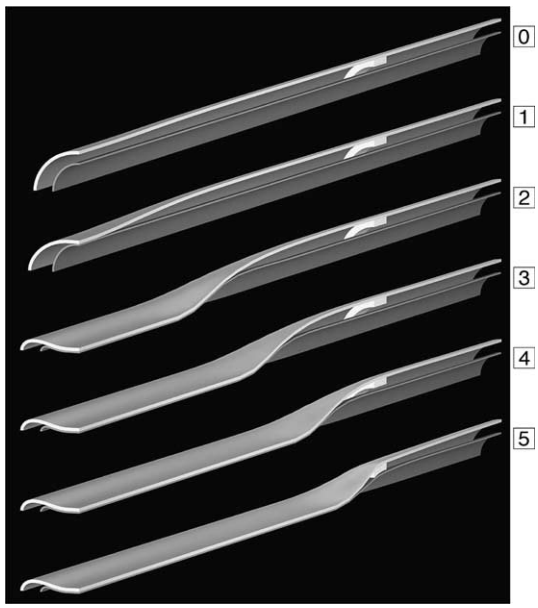

Fig. 17. Sequence of calculated deformed configurations corresponding to points identified on dynamic response in Fig. 15 at $\overline{P}_I = 0.524$.

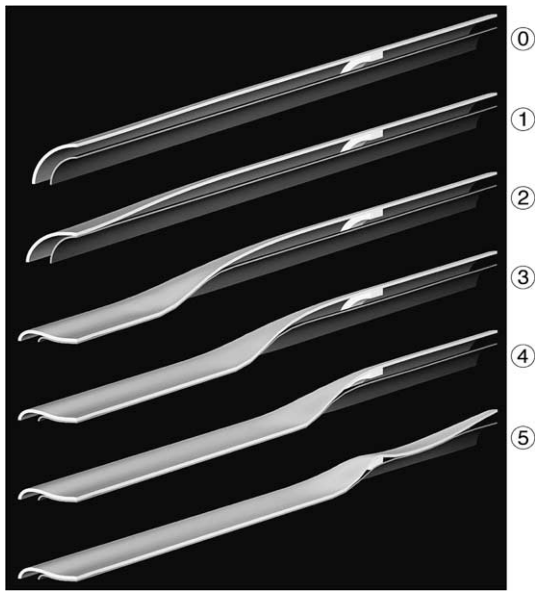

Fig. 18. Sequence of calculated deformed configurations corresponding to points identified on dynamic response in Fig. 15 at $\overline{P}_I = 0.568$.

which of course is higher than the quasi-static value. These values were used in Eq. (2) to bracket the dynamic efficiency in the manner shown under $\hat{\eta}_D$ in Table 8.

Similar dynamic calculations were performed for each of the four arrestors analyzed quasi-statically. The calculated dynamic efficiencies bracketed in a similar manner as above are listed in Table 8. The dynamic efficiencies are plotted against the corresponding quasi-static values in Fig. 19. In all cases the dynamic efficiency is higher than the quasi-static value which is in agreement with the experimental results. We point out that the numerical calculations were not intended to serve as replicas of the experiments, but to

Table 8
Calculated dynamic arrestor efficiencies ($L/D = 0.5$)

h/t	Mode[a]	P_I psi (bar)	$\hat{\eta}_D$
1.8237	–	1200 (82.7)	0.381
1.8237	○	1300 (89.6)	0.438
1.9757	–	1300 (89.6)	0.438
1.9757	○	1400 (96.5)	0.494
2.1277	–	1425 (98.3)	0.509
2.1277	○	1500 (103.4)	0.551
2.2796	–	1600 (110.3)	0.608
2.2796	○	1700 (117.2)	0.665

[a] The symbol (–) indicates that no crossover occurred.

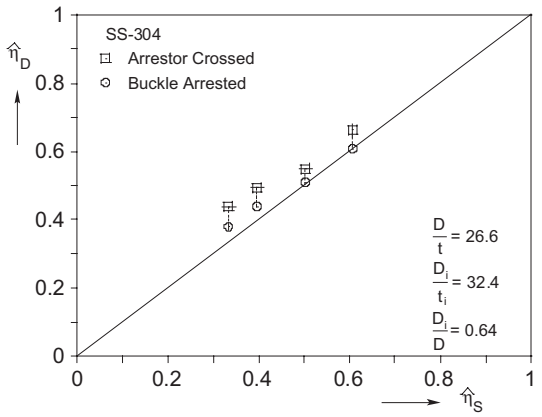

Fig. 19. Dynamic vs. quasi-static arresting efficiencies calculated for three arrestors.

qualitatively reproduce the physical phenomenon, aiming at elucidating the reasons behind the enhancement in the arrestor performance due to dynamics.

This dynamic enhancement in arresting performance was also observed in the case of integral arrestors welded to single pipes (Netto and Kyriakides, 2000a,b). The main contributor to the enhancement was shown to be the dynamic sharpening of the profile of running buckles. This in turn increases the amplitude of the reverse ovality induced just downstream of the propagating buckle front. When the buckle engages the arrestor, the arrestor and a section of the pipe downstream of it experience significantly more reverse ovality than under quasi-static loading. This delays the development of the flattening of both which is the mechanism of crossover preferred by arrestors in this range of pressures. In some cases this may result to the flipping mode of crossover which occurs for higher efficiency arrestors, which again means enhancement in performance. This mode switch was indeed observed in two of the arrestors tested dynamically. As pointed out above, dynamic sharpening of the profile of propagating buckles in pipe-in-pipe systems was found to be comparable to that of single pipes of the same dimensions as the outer pipe. The reverse ovality induced to the downstream pipe was also very similar in magnitude. In the presence of an internal ring arrestor the numerical simulations showed that the interaction of this reverse ovality with the arrestor and the section of pipe adjacent to it lead to a similar reduction of flattening. Thus they collapse at a higher pressure. Because of these similarities between the enhancement mechanisms of the internal ring and the integral arrestors, in the interest of space further supporting evidence will not be provided here. Interested readers are referred to Netto and Kyriakides (2000b) for further details on this subject.

4. Summary and conclusions

The problem of dynamic buckle propagation in pipe-in-pipe systems and its effect on the performance of internal ring buckle arrestors has been studied through a combination of experiment and analysis. The experiments involved seamless stainless steel 304 tubes. The outer tubes had D/t of approximately 27 and the inner ones had D/t of around 32 and 23. For these parameters local collapse and its subsequent propagation result in simultaneous flattening of both pipes very similar to that occurring in single pipes. In dynamic experiments the buckle was initiated at one end of the two-pipe system in a constant pressure environment of either water or air. The buckle localizes, accelerates to steady state in a length of a few pipe diameters, and continues at this velocity to the end of the two-pipe system. The velocity increases with pressure and, in general, is higher in air than in water. The measured velocities were found to follow the

same trends and to be comparable to similar measurements in single tubes with approximately the same geometric and material characteristics as the outer tube.

The dynamic buckle propagation experiments in air were simulated through a finite element model which accounts for the geometric, material and contact nonlinearities as well as for the inertia of the pipes. The structure collapses in vacuum and thus the simulations are considered to be comparable to the experiments in air. The calculated velocities follow the same trend but are somewhat higher than the measured values. The size of the problem is quite significant and the mesh adopted was not optimal resulting in some stiffening of the structure and higher buckle velocities. Increase in pressure (and velocity) was found to cause sharpening of the profile of the buckle. This is accompanied by an increase in the amplitude of reverse ovality just ahead of the profile. Both of these effects are comparable to those seen in single pipes of similar characteristics as the outer one.

In a second phase of the work, the performance of ring buckle arrestors placed in the annulus in close contact with the outer tubes was evaluated under dynamic buckle propagation conditions. The crossover pressure of several arrestors was first established in quasi-static experiments. A series of dynamic tests were performed for each arrestor in which the dynamic crossover pressure was established within about 100 psi ($\sim$7 bar). In all cases the dynamic crossover pressure, and correspondingly the arresting efficiency, were found to be higher than the quasi-static ones. This indicates that design of such devices using the methodology in Olso and Kyriakides (2003), which is based on quasi-static crossover experiments and analyses, should be conservative.

The dynamic arrest experiments were also simulated numerically. The simulations produced a similar dynamic enhancement in arrestor performance as was observed experimentally. The main contributor to the enhanced performance is the dynamic sharpening of the buckle profile and the increase in the amplitude of reverse ovality ahead of it. When a running buckle engages the arrestor and its neighborhood, the arrestor and a section of the pipe downstream of it experience significantly more reverse ovality than under quasi-static loading. This delays the development of the flattening of both, which is the mechanism of crossover preferred by arrestors for most of the pressure range of interest. The net effect is that a higher pressure is required to cross the arrestor in the flattening mode. Above some pressure levels this can result in a switch from the flattening to the flipping mode of crossing as was observed in two of the experiments.

Acknowledgements

The work presented was conducted with the financial support of a consortium of industrial sponsors. The work of TAN was also sponsored by CNPq–Brazil. The authors wish to thank Robert D. Cook for assistance in the execution of the experiments and L.-H. Lee for help in rendering the calculated pipe collapse configurations.

References

Dyau, J.-Y., Kyriakides, S., 1993. On the propagation pressure of long cylindrical shells under external pressure. International Journal of Mechanical Sciences 35, 675–713.

Hilber, H.M., Hughes, T.J.R., Taylor, R.L., 1977. Improved numerical dissipation for time integration algorithms in structural dynamics. Earthquake Engineering and Structural Dynamics 5, 283–292.

Hilber, H.M., Hughes, T.J.R., 1978. Collocation, dissipation and "overshoot" for time integration schemes in structural dynamics. Earthquake Engineering and Structural Dynamics 6, 99–117.

Johns, T.G., Mesloh, R.E., Sorenson, J.E., 1978. Propagating buckle arrestors for offshore pipelines. ASME Journal of Pressure Vessel Technology 100, 206–214.

Kyriakides, S., Corona, E., Dyau, J.-Y., 1994. Pipe collapse under bending, tension, and external pressure (BEPTICO). Computer Program Manual, EMRL Report, No. 94/4.

Kyriakides, S., 2002a. Efficiency limits for slip-on type buckle arrestors for offshore pipelines. ASCE Journal of Engineering Mechanics 128, 102–111.

Kyriakides, S., 2002b. Buckle propagation in pipe-in-pipe systems. Part I Experiments. International Journal of Solids and Structures 39, 351–366.

Kyriakides, S., Babcock, C.D., 1979. On the dynamics and the arrest of the propagating buckle in offshore pipelines. In: Proc. Offshore Techn. Conference, OTC 3479, pp. 1035–1045.

Kyriakides, S., Babcock, C.D., 1980. On the 'slip-on' buckle arrestor for offshore pipelines. ASME Journal of Pressure Vessel Technology 102, 188–192.

Kyriakides, S., Park, T.-D., Netto, T.A., 1997. On the design of integral buckle arrestors for offshore pipelines. In: Vugts, J.H. (Ed.), Proc. BOSS'97, vol. 1. Pergamon (Elsevier Sciences), pp. 277–289. Also, Applied Ocean Research 20, 95–114, 1998.

Kyriakides, S., Netto, T.A., 2000. On the dynamics of propagating buckles in pipelines. International Journal of Solids and Structures 37, 6843–6867.

Kyriakides, S., Netto, T.A., 2002. Dynamic propagation and arrest of buckles in pipe-in-pipe systems. In: Proc. Offshore Mechanics and Arctic Engineering '02, Oslo, Norway, June 2002.

Kyriakides, S., Vogler, T.J., 2002. Buckle propagation in pipe-in-pipe systems. Part II Analysis. International Journal of Solids and Structures 39, 367–392.

Langner, C.G., 1999. Buckle arrestors for deepwater pipelines. In: Proc. Offshore Techn. Conference, OTC Paper 10711 3, pp. 17–28.

Netto, T.A., Kyriakides, S., 2000a. Dynamic performance of integral buckle arrestors for offshore pipelines. Part I Experiments. International Journal of Mechanical Sciences 42, 1405–1423.

Netto, T.A., Kyriakides, S., 2000b. Dynamic performance of integral buckle arrestors for offshore pipelines. Part II Analysis. International Journal of Mechanical Sciences 42, 1425–1452.

Olso, E., Kyriakides, S., 2003. Internal ring buckle arrestors for pipe-in-pipe systems. International Journal of Nonlinear Mechanics 38, 1267–1284.

Park, T.-D., Kyriakides, S., 1997. On the design of integral buckle arrestors for offshore pipelines. International Journal of Mechanical Sciences 39, 643–669.